Local Vibrations and Negative Thermal Expansion in ZrW_2O_8

F. Bridges,[1] T. Keiber,[1] P. Juhas,[2] S. J. L. Billinge,[2,3] L. Sutton,[1] J. Wilde,[1] and Glen R. Kowach[4]
[1]*Department of Physics, University of California, Santa Cruz, California 95064, USA*
[2]*Condensed Matter Physics and Materials Science Department, Brookhaven National Laboratory, Upton, New York 11973, USA*
[3]*Department of Applied Physics and Applied Mathematics, Columbia University, New York, New York 10027, USA*
[4]*Department of Chemistry, The City College of New York, The City University of New York, New York, New York 10031 USA*
(Received 17 September 2013; published 28 January 2014)

We present an x-ray pair distribution function (XPDF) analysis and extended x-ray absorption fine structure (EXAFS) data for ZrW_2O_8 (10–500 K) with a focus on the stiffness of the Zr-O-W linkage. The XPDF is highly sensitive to W-Zr and W-W correlations, but much less so to O-O or W-O correlations. The Zr-W peak in the XPDF data has a weak temperature dependence and, hence, this linkage is relatively stiff and does not permit bending of the Zr-O-W link. We propose that the low energy vibrational modes that lead to negative thermal expansion involve correlated rotations of ZrO_6 octahedra that produce large $\langle 111 \rangle$ translations of the WO_4 tetrahedra, rather than a transverse motion of O atoms that imply a flexible Zr-O-W linkage.

DOI: 10.1103/PhysRevLett.112.045505 PACS numbers: 61.05.cj, 65.40.De

Although most materials expand with increasing temperature T, a small number of compounds, many with complex structures, contract over a wide temperature range; that unusual behavior has attracted considerable attention [1–19]. In several recent reviews [17–19] (and references therein) the assumed mechanism when lattice vibrations produce negative thermal expansion (NTE) is always a transverse motion of the central O atom in a nearly linear M-O-M' linkage as for fluorine in ScF_3 [20,21]. ZrW_2O_8 is the archetype of one family of such compounds and exhibits NTE from 10–1000 K [2,5]. The phonon energies span a large energy range, from ~1500 K (125 meV) for the W-O stretching modes [22,23], to low energy optical phonon bands (38 and 67 K), observed in both neutron scattering [4,7] and specific heat measurements [6]. The latter modes also have a negative Grüneisen parameter [4,7,11], and their low energy explains why a significant NTE is observed at 15 K. These materials also have a very low thermal conductivity [15,16], which is likely a result of the very low energy optical modes, similar to the "rattler" modes in clathrates and skutterudites [24,25]. The crystal lattice for ZrW_2O_8 below ~420 K (space group $P2_13$) is an open structure formed of corner-linked ZrO_6 octahedra and WO_4 tetrahedra (see Fig. 1 and the Supplemental Material [26]). The latter occur in pairs, $W1O_4$ and $W2O_4$, with one vertex oriented along $\langle 111 \rangle$ axes [3,5,8]. The apical O3 and O4 atoms are only bonded to W and the WO_4 tetrahedra can, therefore, translate into voids along the $\langle 111 \rangle$ axis.

NTE is generally attributed to anharmonic vibrations that reduce the void volume. However, the low energy vibrations in ZrW_2O_8 are poorly understood and there are competing models [12–14,27]. Tucker *et al.* [13] assumed that the important vibration modes leading to NTE involve rigid rotations of the vertex-linked polyhedral units, and used the rigid unit mode (RUM) model [28] in a reverse Monte Carlo (RMC) analysis of their neutron pair distribution function (NPDF) data. This lead to large transverse vibrations of O and is often cited as evidence that the transverse vibration model applies to NTE in ZrW_2O_8. However, a focus on only correlated rotations ignores the possibility of WO_4 translations.

In an earlier report Cao *et al.* [12] noted the large amplitude vibration for W1-W2 pair (i.e., translations of the rigid $W1O_4$ and $W2O_4$ tetrahedra along the $\langle 111 \rangle$ axes) that is observed in both EXAFS [12,27] and NPDF measurements [13,14], and also reported that the Zr-O-W linkage is remarkably stiff. Based on these two results

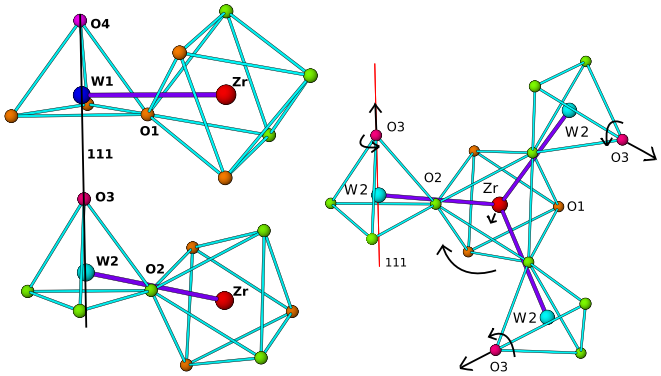

FIG. 1 (color online). An expanded view of the relationship between the WO_4 tetrahedra and the ZrO_6 octahedra. The W1-O1-Zr linkage has an angle of ~155°, while the W2-O2-Zr linkage is nearly collinear (173°). Left: only one of the three ZrO_6 octahedra connected to the WO_4 tetrahedra via O1 or O2 is shown. Right: if a ZrO_6 octahedron rotates about a $[11\bar{1}]$ axis (out of the page) each of the connected $W2O_4$ tetrahedra rotate in a similar manner with a translation along another $\langle 111 \rangle$ axis, with a small rotation about that axis as shown.

they argued that NTE arises from a correlated translation of the WO_4 units together with rotations of the ZrO_6 units that move the Zr atoms together. These correlated translational-rotational motions do not flex the Zr-O-W linkages significantly, and most of the O2 and O1 motions observed in diffraction studies, i.e., the thermal parameters [3,5] are associated with the translations of the WO_4 units. The connectivity of the lattice, in fact, requires that the tetrahedra both translate and rotate (slightly) as the lattice contracts [3,29].

Because there are complications with both analyses, this conflict is not easily resolved. In the NPDF data, the Zr-W peak amplitude is very small and W-O and O-O pair correlations overlap. For the EXAFS data there are also W1-O1-Zr and W2-O2-Zr multiscattering peaks, which must also be fit. However, it is not obvious how the multiscattering peaks could lead to a weak T dependence for the W-Zr (or Zr-W) peak in both the W L_{III} and Zr K edge data.

To resolve the conflicts described above we have carried out a joint x-ray pair distribution function (XPDF) analysis and EXAFS study on a new ZrW_2O_8 sample specially prepared to have no pressure induced phase—see details in the Supplemental Material [26]. The XPDF is not very sensitive to oxygen correlations (except for the nearest W-O pairs), but is highly sensitive to the metal-metal correlations, W-W, W-Zr, etc. Consequently for the W-Zr peaks any overlapping O-O correlations are negligible and other W-O correlations small. We have also extended the temperature range up to 500 K for both measurements, but restrict the discussion here to temperatures below the order-disorder transition near 425 K [3]. Much of the focus is on the stiffness of the W-Zr pairs.

The XPDF experiments were carried out at the Advanced Photon Source (APS), beam line 11-ID-C, using 115 keV x rays; the x-ray beam was 0.85×0.85 mm^2. The powdered sample was mounted in a 1 mm diameter Kapton tube and the tube was rocked $\pm 5^{\circ}$ along its axis to improve powder averaging. The temperature was ramped slowly from low to high temperature and several 2D powder diffraction patterns were collected per every 1 K interval. The 2D plots were reduced using the program FIT2D [30], and then 9–10 files were averaged (within a ± 1.7 K range) to improve the signal-to-noise ratio. The averaged powder patterns were converted to the pair distribution function $G(r)$ using PDFGETX3 [31], with $Q_{\mathrm{max}} = 26$ Å^{-1}. For comparison with the EXAFS data, the $G(r)$ curves were converted to a radial distribution function $R(r)$, $[R(r) = r(G(r) + 4\pi r \rho_0)]$, where ρ_0 is nominally the atom number density, although, in practice, ρ_0 is adjusted to make a flat baseline in $R(r)$ at low r.

The EXAFS experiments were carried out at the Stanford Synchrotron Radiation Lightsource (SSRL) on beam line 10-2, using (220) monochromator crystals; the powdered sample was mounted on tape. A helium cryostat was used from 4–330 K while a small oven was used from 300–560 K. See the Supplemental Material [26] for further details. The suite of programs in RSXAP [32] were used to reduce and analyze the EXAFS data; this analysis and fit of the r-space data is similar to that described earlier [12,27].

In Fig. 2 we plot the XPDF $R(r)$ for different values of T for the low r range 1.5 to 5.25 Å. Here the W-O peak (sum of four peaks) is at 1.8 Å, the weaker Zr-O peak (sum of two peaks) is at 2.1 Å, the W-Zr peak (sum of W1-Zr and W2-Zr) is near 3.8 Å, the first W1-W2 peak is near 4.1 Å, and a second W-W correlation is near 4.65 Å. At low T there is also a weak W-O peak near 4.35 Å. Our attention here is focused on the temperature dependencies. The relatively weak W-O and Zr-O peaks at low r show no significant T dependence. The most dramatic temperature response occurs for the W1-W2 peaks at 4.12 and 4.65 Å; they broaden and decrease in amplitude from 10 to 300 K, to ~70% of the original height. For temperatures above ~350–400 K, the 4.12 Å peak becomes locked and the amplitude changes little (drops to ~66% at 490 K), while the 4.65 Å peak develops a small shoulder at 4.45 Å and the amplitude drops further to 54%—see the inset in Fig. 2. This peak arises from three neighbors; at high T the shoulder, which corresponds to approximately one neighbor, is shifted to lower r, suggesting a symmetry breaking —but that is beyond the scope of this Letter. In contrast the T dependence for the Zr-W peak is surprisingly weak—much weaker than all other metal-metal peaks. It is very unusual to have two peaks so close together (3.85 and 4.12 Å) with such different dynamics [33].

In Fig. 3, we plot the corresponding k^2 weighted EXAFS for the W L_{III} and Zr K edges. For the W L_{III} edge, the nearest neighbor W-O peak near 1.4 Å is very large compared to peaks for more distant neighbors;

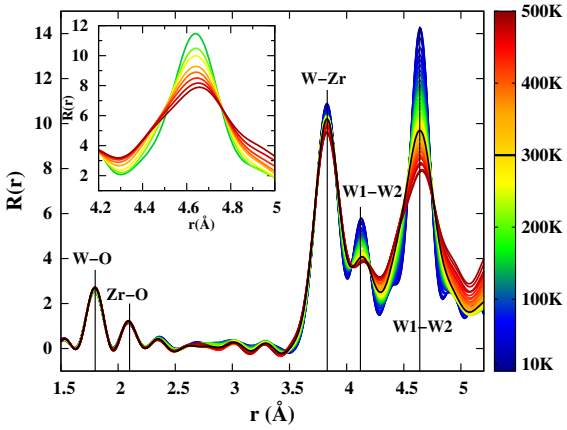

FIG. 2 (color online). XPDF radial distribution function $R(r)$ as a function of T from 10–500 K. W-O peak, 1.8 Å; Zr-O peak, 2.1 Å; Zr-W1,2 peak, 3.8 Å; first W1-W2 peak (pair along a ⟨111⟩ axis), 4.12 Å; and the further W-W correlation peak, 4.65 Å. Inset: expanded view of the 4.65 Å peak showing a splitting above 390 K. The black line corresponds to 300 K.

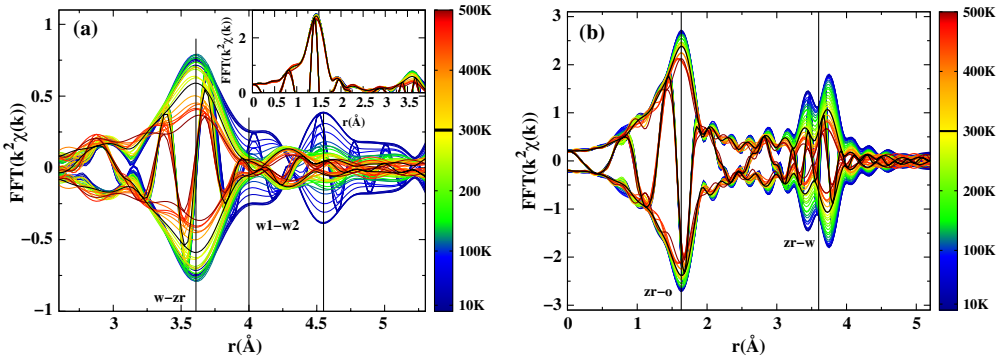

FIG. 3 (color online). EXAFS r-space data (FFT$[k^2\chi(k)]$) for (a) the W L_{III} and (b) the Zr K edge as a function of T from 10–500 K; the 300 K trace is shown as black. The fast Fourier transform (FFT) ranges are W, 3.8–14.5 Å^{-1}; Zr, 3.7–16.4 Å^{-1}, Gaussian rounded by 0.2 Å^{-1}. The fast oscillating function is the real part Re of the FFT while the envelope is $\pm\sqrt{\mathrm{Re}^2+\mathrm{Im}^2}$, where Im is the imaginary part of the FFT. The first W-O peak is shown in the inset: it occurs near 1.4 Å and is roughly 3 times larger than the W-Zr peak at 3.6 Å.

consequently we plot the r-space data on an expanded scale from 2.6–5.3 Å, to show the W-Zr peak near 3.6 Å and the W1-W2 peak near 4.0 Å (a shoulder on the Zr-W peak). The peak near 4.6 Å is another W-W peak (Note that there is a small (known) r shift of each EXAFS peak to lower r). The first W-O peak (see the inset) has a very weak T dependence in agreement with the XPDF data and indicates extremely stiff W-O bonds.

The Zr-O peak near 1.7 Å [Fig. 3(b)] also has a weak temperature dependence, but stronger than for W-O, indicating moderately strong bonds. The Zr-W peaks are spread over 3.4–3.8 Å; part of the complex shape for these peaks arises from multiple scattering effects; the apparent peak near 3.4 Å is mainly from a multiple scattering component and the dip near 3.6 Å is from destructive interference between the single scattering Zr-W and multi-scattering Zr-O-W contributions.

The XPDF data $R(r)$ were fit from 3.0–4.8 Å using four Gaussians for (1) the overlapping Zr-W1,2 peaks near 3.8 Å, (2) the first W1-W2 peak at 4.12 Å, (3) the second W-W peak at 4.65 Å, and (4) at low T, a weak W-O peak near 4.35 Å. An example of the fit at 10 K is shown in Fig. 4. From fits of several low T scans we obtained the average amplitude for each peak, which was then fixed for fits of the higher T data to obtain the width σ as a function of T. Similar quality fits were obtained at higher temperatures, but the weak W-O peak (4.35 Å) broadens rapidly as seen in Fig. 2. For later σ^2 plots we assumed $\sigma_{\mathrm{Zr-W1}} = \sigma_{\mathrm{Zr-W2}}$ and removed the effect of the splitting of the Zr-W1 and Zr-W2 peaks ($\Delta r \sim 0.125$ Å [3]) following Teo [34].

The difference between the data and fit, shown as solid circles below the data in Fig. 4, is small, but suggests that several small peaks are missing that are close to the positions of weak W-O correlations based on the structure [3]; two are located near the Zr-W peak (see black vertical lines). We, therefore, carried out some constrained fits at low T, which included the small peaks on each side of the Zr-W peak; the positions were constrained to the structure [3] and the amplitudes were 1/3 that of the weak W-O peak at 4.35 Å, again from the structure [3]. These fits show that ignoring the weak W-O peaks at low T effectively broadens the Zr-W1,2 peak; the decrease in σ^2 for the Zr-W peak from this effect is about 0.001–0.002 Å^2; see the solid black square on Fig. 5. Unfortunately, similar fits at higher temperatures were unstable.

Fits of the EXAFS data—W L_{III} (W-O, W-Zr, W1-W2) and Zr K edge (Zr-O, Zr-W)—were carried out in r space using theoretical functions from FEFF [35]. Here we first fit the O-neighbor peak (fit ranges: 1.2–1.7 Å for the W L_{III} edge and 1.4–1.9 Å for the Zr K edge) using four W-O and two Zr-O peaks with the amplitudes and relative positions constrained to the structure [3]; one average distance was allowed to vary for each edge. We also assumed that the four unresolved W-O peaks had the same σ and similarly for the two unresolved Zr-O peaks. From fits of the O-neighbor peaks at low T, the value of S_o^2 was

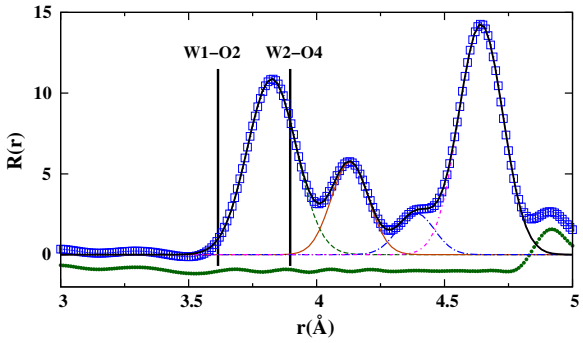

FIG. 4 (color online). Fit of the XPDF function $R(r)$ (blue square) at 10 K, from 3.0–4.8 Å, to a sum of four peaks: Zr-W (3.8 Å), W1-W2 (4.12 Å), long W-W (4.65 Å), and a weak W-O peak near 4.35 Å. The individual peaks are shown as well as the total fit (solid black line). The difference (data − fit) is shown as small dark circles, offset by −0.2 on the y axis.

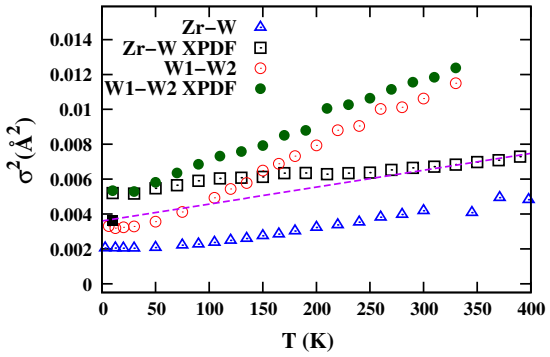

FIG. 5 (color online). $\sigma^2(T)$ for the W1-W2 and Zr-W peaks from EXAFS and XPDF data. The solid black square is the fit when two weak W-O peaks near 3.65 and 3.9 Å are included at 10 K in fits of $R(r)$. The dotted line is the expected behavior for the Zr-W peak in the XPDF data when the effects of W-O are removed.

0.99 for both the W and Zr edges. Values of $\sigma^2(T)$ for these W-O and Zr-O peaks agree well with the previous EXAFS data [12,27] as well as the theoretical values for Zr-O from Vila *et al.* [36]. See the Supplemental Material [26] for details.

To include further neighbors in the W L_{III} edge data (3.2–4.6 Å) we used two W1,2-Zr peaks, two W1,2-O-Zr multiscattering peaks, a W1-W2 peak, and its corresponding multiscattering peak W1-O3-W2, plus a longer W-W peak to provide the "tail" under the W1-W2 peak. The W1,2-Zr peaks could not be uniquely resolved [26]; consequently, the relative distances and amplitudes of the W1-Zr, W2-Zr, W1,2-O-Zr multiscattering peaks, and also the W1-W2 peak were constrained to the structure [3], with the value of σ for the two W1,2-Zr and W1,2-O-Zr peaks set equal. For the Zr K edge data we fit the Zr-W1,2 peak over the range 3.3–4.3 Å. See the Supplemental Material [26] for further details. In Fig. 5 we plot σ^2 for the Zr-W and W1-W2 atom pairs obtained from the XPDF and EXAFS results—the results are quite similar, although there is a larger static offset for the XPDF result; most importantly σ^2 for the Zr-W peak remains small indicating a stiff Zr-O-W linkage. A comparison with earlier data is included in the Supplemental Material [26].

To understand how correlated translational-rotational motions occur when the Zr-O-W linkages are stiff, consider the substructures of the unit cell in Fig. 1. The left side shows two tetrahedra $W1O_4$ and $W2O_4$ that are aligned along a [111] axis; this axis is tilted slightly out of the page by $\sim 20^{\circ}$. We now focus on displacements of a $W2O_4$ tetrahedron; those for $W1O_4$ are similar. The structure on the right-hand side shows that a clockwise rotation of a ZrO_6 octahedron about a $[11\bar{1}]$ axis (out of the page), produces a vertical displacement of the O2 atom on the left. Because the [111] axis tilts only slightly out of the page the component of this displacement along [111] is large, and together with correlated motions of two other ZrO6, produces the large $W2O_4$ translation. However the small tilt also produces a small component perpendicular to the [111] axis (smaller by a factor of 3), which leads to a small rotation of the $W2O_4$ about [111]. The other two $W2O_4$ tetrahedra shown in Fig. 1 (right) are equivalent under threefold rotation symmetry. Evans *et al.* [3] noted that the ZrO_6 octahedra rotated about the $\langle 111 \rangle$ axes but did not consider components.

Next consider an upward translation of the $W2O_4$ tetrahedron in light of the stiff, nearly collinear W2-O-Zr linkage; the three Zr neighbors must move toward the [111] axis on average, and hence toward each other. This model can be considered an extension of the RUM model with a significant translational motion of one of the rigid units also included. The large translational motions of the WO_4 tetrahedra, driven by correlated rotations of the three connected ZrO_6 octahedra, are possible because the O3 and O4 vertices are not bonded to other atoms.

In summary, there is good agreement between the XPDF and EXAFS results for the strongest peaks, up to ~5 Å, when $T < 400$ K. A major result is that the peak for the shortest W1,2-Zr pairs has a surprisingly weak temperature dependence indicating stiff W-O-Zr linkages, consistent with Ref. [12]; this temperature dependence is comparable in the XPDF and EXAFS data. For the XPDF data, other overlapping peaks are small and have a small effect on the W1,2-Zr pair. This weak dependence agrees well with the earlier EXAFS results but it casts doubt on any interpretation of the NTE in terms of RUMs involving only large transverse motion of O within the Zr-O-W2 linkage [13,14].

The resulting correlated translational-rotational motions are much more complex than rotations of neighboring polyhedra used in simple RUM models; the translational vibration of the W1-W2 pair (two WO_4 tetrahedra vibrating along the [111] axis) involves correlated rotations of at least six ZrO_6 octahedra, plus translations of several other WO_4 tetrahedra, which connect the ZrO_6 octahedra. The vibrating linkage may extend outside the unit cell. The most important result is that unlike all other phonon models for NTE which assume a large transverse motion of a corner-linking atom, the correlated translational-rotational motions described above decrease void volume by translation of WO_4 units into empty space without a significant transverse motion of corner-linking atoms. This model may apply to other open crystal lattices.

The EXAFS work (performed by F. B. and T. K.) was supported under NSF Grant No. DMR1005568. The experiments were performed at SSRL, operated by the U.S. DOE, Division of Chemical Sciences. The XPDF experiments were performed at the APS, Argonne National Laboratories, operated for the U.S. Department of Energy, Office of Science (U.S. DOE-OS), by Argonne National Laboratory under Contract No. DE-AC02-06CH11357. The work of S. J. L. B. and P. J. at the Brookhaven

National Laboratory is supported by U.S. DOE-OS Contract No. DE-AC02-98CH10886. F. B. thanks I. Levin for helpful discussions and Rob Heffern for help in the initial EXAFS analysis of the W-O and Zr-O pairs.

[1] C. Martinek and F. A. Hummel, J. Am. Ceram. Soc. **51**, 227 (1968).
[2] T. A. Mary, J. S. O. Evans, T. Vogt, and A. W. Sleight, Science **272**, 90 (1996).
[3] J. S. O. Evans, T. A. Mary, T. Vogt, M. A. Subramanian, and A. W. Sleight, Chem. Mater. **8**, 2809 (1996).
[4] W. I. F. David, J. S. O. Evans, and A. W. Sleight, Europhys. Lett. **46**, 661 (1999).
[5] J. S. O. Evans, W. I. F. David, and A. W. Sleight, Acta Crystallogr. Sect. B **55**, 333 (1999).
[6] A. P. Ramirez and G. R. Kowach, Phys. Rev. Lett. **80**, 4903 (1998).
[7] G. Ernst, C. Broholm, G. R. Kowach, and A. P. Ramirez, Nature (London) **396**, 147 (1998).
[8] J. D. Jorgensen, Z. Hu, S. Teslic, D. N. Argyriou, S. Short, J. S. O. Evans, and A. W. Sleight, Phys. Rev. B **59**, 215 (1999).
[9] R. Mittal and S. L. Chaplot, Phys. Rev. B **60**, 7234 (1999).
[10] R. Mittal and S. L. Chaplot, Solid State Commun. **115**, 319 (2000).
[11] R. Mittal, S. L. Chaplot, H. Schober, and T. A. Mary, Phys. Rev. Lett. **86**, 4692 (2001).
[12] D. Cao, F. Bridges, G. R. Kowach, and A. P. Ramirez, Phys. Rev. Lett. **89**, 215902 (2002).
[13] M. G. Tucker, A. L. Goodwin, M. T. Dove, D. A. Keen, S. A. Wells, and J. S. O. Evans, Phys. Rev. Lett. **95**, 255501 (2005).
[14] M. G. Tucker, D. A. Keen, J. S. O. Evans, and M. T. Dove, J. Phys. Condens. Matter **19**, 335215 (2007).
[15] C. A. Kennedy and M. A. White, Solid State Commun. **134**, 271 (2005).
[16] C. A. Kennedy, M. A. White, A. P. Wilkinson, and T. Varga, Appl. Phys. Lett. **90**, 151906 (2007).
[17] W. Miller, C. W. Smith, D. S. Mackenzie, and K. E. Evans, J. Mater. Sci. **44**, 5441 (2009).
[18] K. Takenaka, Sci. Tech. Adv. Mater. **13**, 013001 (2012).
[19] C. Lind, Materials **5**, 1125 (2012).
[20] B. K. Greve, K. L. Martin, P. L. Lee, P. J. Chupas, K. W. Chapman, and A. P. Wilkinson, J. Am. Chem. Soc. **132**, 15496 (2010).
[21] C. W. Li, X. Tang, J. A. Munoz, J. B. Keith, S. J. Tracy, D. L. Abernathy, and B. Fultz, Phys. Rev. Lett. **107**, 195504 (2011).
[22] T. R. Ravindran, A. K. Arora, and T. A. Mary, J. Phys. Condens. Matter **13**, 11573 (2001).
[23] C. Pantea, A. Migliori, P. B. Littlewood, Y. Zhao, H. Ledbetter, J. C. Lashley, T. Kimura, J. Van Duijin, G. R. Kowach, Phys. Rev. B **73**, 214118 (2006).
[24] B. C. Sales, B. C. Chakoumakos, R. Jin, J. R. Thompson, and D. Mandrus, Phys. Rev. B **63**, 245113 (2001).
[25] B. C. Sales, in *Handbook on the Physics and Chemistry of Rare Earths*, edited by L. Eyring, K. A. Gschneidner, and G. H. Lander (Elsevier, New York, 2002), Vol. 33, pp. 1–34.
[26] See Supplemental Material at http://link.aps.org/supplemental/10.1103/PhysRevLett.112.045505 for additional figures and experimental details.
[27] D. Cao, F. Bridges, G. R. Kowach, and A. P. Ramirez, Phys. Rev. B **68**, 014303 (2003).
[28] A. K. A. Pryde, K. D. Hammonds, M. T. Dove, V. H. J. D. Gale, and M. C. Warren, J. Phys. Condens. Matter **8**, 10973 (1996).
[29] J. N. Hancock, C. Turpen, Z. Schlesinger, G. R. Kowach, and A. P. Ramirez, Phys. Rev. Lett. **93**, 225501 (2004).
[30] A. P. Hammersley, ESRF Internal Report No. ESRF98-HA01T, 2004 (unpublished).
[31] P. Juhas, T. Davis, C. L. Farrow, and S. J. L. Billinge, J. Appl. Crystallogr. **46**, 560 (2013).
[32] C. H. Booth, R-Space X-ray Absorption Package, http://lise.lbl.gov/RSXAP/.
[33] I.-K. Jeong, T. Proffen, F. Mohiuddin-Jacobs, and S. J. L. Billinge, J. Phys. Chem. A **103**, 921 (1999).
[34] B. K. Teo, *EXAFS: Basic Principles of Data Analysis* (Springer-Verlag, New York, 1986).
[35] A. L. Ankudinov, B. Ravel, J. J. Rehr, and S. D. Conradson, Phys. Rev. B **58**, 7565 (1998).
[36] F. D. Vila, V. E. Lindahl, and J. J. Rehr, Phys. Rev. B **85**, 024303 (2012).